Advances in Electrochemical Science and Engineering

Volume 8

Edited by Richard C. Alkire
and Dieter M. Kolb

Contributions from

J. Fleig, Stuttgart
K. Krischer, Berlin
Y. V. Pleskov, Moskow
H.-H. Strehblow, Düsseldorf

WILEY-VCH

Advances in Electrochemical Science and Engineering

Volume 8

Advances in Electrochemical Science and Engineering

In collaboration with the International Society of Electrochemistry

Advances in Electrochemical Science and Engineering

Volume 8

Edited by Richard C. Alkire
and Dieter M. Kolb

Contributions from

J. Fleig, Stuttgart
K. Krischer, Berlin
Y. V. Pleskov, Moskow
H.-H. Strehblow, Düsseldorf

WILEY-VCH

Editors:
Prof. Richard C. Alkire
University of Illinois
600 South Mathews Avenue
Urbana, IL 61801
USA

Prof. Dieter M. Kolb
University of Ulm
Department of Electrochemistry
Albert-Einstein-Allee 47
89081 Ulm
Germany

Library of Congress Card No.: applied for

A catalogue record for this book is available from the British Library.

Bibliographic information published by Die Deutsche Bibliothek
Die Deutsche Bibliothek lists this publication in the Deutsche Nationalbibliografie; detailed bibliographic data is available in the Internet at http://dnb.ddb.de

ISBN 3-527-30211-5

Composition: Asco Typesetters, Hong Kong.
Printing: betz-druck gmbh, Darmstadt.
Bookbinding: J. Schäffer GmbH & Co. KG, Grünstadt.
Printed in the Federal Republic of Germany.

Introduction

This eighth volume continues the series established by the late Heinz Gerischer and Charles W. Tobias. The favourable reception of the first seven volumes and the steady increase of interest in electrochemical science and technology provide good reasons for the continuation of this series with the same high standards. The purpose of the series is to provide high quality advanced reviews of topics of both fundamental and practical importance for the experienced reader.

Richard C. Alkire
Dieter M. Kolb

Preface

Fleig reviews fundamental aspects of solid state ionics, and illustrates many similarities between the field of solid state electrochemistry and liquid electrochemistry. These include the consideration of mass and charge transport, electrochemical reactions at electrode/solid interfaces, and impedance spectroscopy. Recent advances in microelectrodes based on solid state ionics are reviewed, along with their application to measuring inhomogeneous bulk conductivities, grain boundary properties, and electrode kinetics of reactions on anion conductors.

Krischer describes in detail the use of nonlinear dynamics in simulating the behavior of systems that can spontaneously form patterns in time and/or space. The discussion illustrates the underlying principles of how such patterns emerge owing to the interplay of homogeneous dynamics and coupling with electrode kinetics, migration, conductivity, cell geometry, and the external circuit. The wide variety of electrochemical systems that give patterns has led to their wide use as convenient "model systems" for exploring fundamentals of nonlinear phenomena. Such knowledge may eventually lead to applications that depend upon controlled instability for useful purposes such as (temporal) catalyst regeneration or (spatial) self-assembly and pattern formation.

The overview by Pleskov covers the literature on electrochemical behavior of synthetic diamond films, as well as the use of electrochemical methods in their characterization. The rapid advancement of the field of diamond electrochemistry was triggered by progress in the technology of deposition of polycrystalline diamond thin films on diamond and other substrates. Advances around the world have by now led to formation of a self-consistent, but as yet incomplete, view of electrochemical behavior of diamond. While discrepancies and scatter between data from different research groups still exist, the rapid advance in film quality and in reliable methods of evaluation point to a promising future.

In the last chapter, Strehblow provides a review of experimental methodology and theoretical concepts of passivation and passivity of metals. The topics of emphasis include growth and composition of passive layers, their structure and electronic properties, and their breakdown. Current accomplishments are discussed in detail for a selected number of key metal and alloy systems. Summarized in some detail are the most important analytical methods for elucidation of chemical composition, electronic properties and structure of passive layers. It is shown for many systems that the application of multiple combinations of electrochemical and spectroscopic methods provide many insights and confidence in the interpretation of the passive behavior of metals.

Contents

List of Contributors

Jürgen Fleig
Max-Planck-Institute for Solid State Research
Heisenbergstr. 1
D-70569 Stuttgart
Germany
juergen.fleig@mpg.de

Katharina Krischer
Fritz-Haber-Institut der Max-Planck-Gesellschaft
Faradayweg 4–6
D-14195 Berlin
Germany
krischer@ph.tum.de

Yuri V. Pleskov
A. N. Frumkin Institute of Electrochemistry
Russian Academy of Sciences
Leninsky Prospekt 31
117071 Moscow
Russia
Pleskov@electrochem.msk.ru

Hans-Henning Strehblow
Institut für Physikalische Chemie und Elektrochemie
Heinrich-Heine-Universität
Universitätsstr. 1
D-40225 Düsseldorf
Germany
Henning@uni-düsseldorf.de

Microelectrodes in Solid State Ionics

Jürgen Fleig

Max–Planck–Institute for Solid State Research, Heisenbergstr. 1, D-70569 Stuttgart, Germany

Contents

List of Symbols

A	area
A_{gb}	grain boundary area
A_{in}	area of the electrochemically inactive (inner) part of a microelectrode
A_{ring}	area of the electrochemically active ring at the three-phase boundary of a microelectrode
b_{ring}	width of the electrochemically active zone at a three-phase boundary
c	concentration
c_{def}	defect concentration
c_{dop}	dopant concentration
c_e	electron concentration
c_h	hole concentration
c_V	vacancy concentration
C	capacitance
C_{bulk}	bulk capacitance
C_{el}	electrode capacitance
C_{gb}	grain boundary capacitance
$\tilde{C}_{in}$	area-related (specific) capacitance of the electrochemically inactive (inner) part of a microelectrode
C_{in}	nominal capacitance of the electrochemically inactive (inner) part of a microelectrode ($\tilde{C}_{in}A_{in}$)
$\tilde{C}_{ring}$	area-related (specific) capacitance of the electrochemically active ring at the three-phase boundary of a microelectrode
C_{ring}	nominal capacitance of the electrochemically active ring at the three-phase boundary of a microelectrode ($\tilde{C}_{ring}A_{ring}$)
C_{spr}	spreading capacitance
C_{stray}	stray capacitance
$\tilde{D}$	chemical diffusion coefficient
d_{me}	microelectrode diameter
e	elementary charge
E	electrical field
Δg	free formation enthalpy of a defect pair
Δh	formation enthalpy of a defect pair
h_R	resistance correction factor
h_C	capacitance correction factor
I	current
$\mathbf{J}$	particle flux
$\mathbf{j}$	current density
k	Boltzmann constant

K	thermodynamic equilibrium constant
L	length (thickness) of a sample
L_g	grain size
LSM	Sr-doped lanthanum manganite
$p(O_2)$	oxygen partial pressure
r	radius
R	resistance
R_{bulk}	bulk resistance
R_{el}	electrode resistance
$\tilde{R}_{el}$	area-related (specific) electrode resistance
$\tilde{R}_{el}^{eff}$	effective area-related (specific) electrode resistance ($R_{el}^{eff} A_{el}$)
R_{el}^{eff}	effective (i.e. measured or simulated) electrode resistance
R_{gb}	grain boundary resistance
$R_{gb,c}$	grain boundary resistance between two large contact electrodes
$R_{gb,me}$	grain boundary resistance between two microelectrodes
R_{spr}	spreading resistance
$R_{\Delta cc}$	additional bulk resistance due to current constriction close to the three-phase boundary
R_{ongb}	resistance measured with a microelectrode on a grain boundary
$R_{ongrain}$	resistance measured with a microelectrode on a grain
$\tilde{R}_{ring}$	area-related (specific) resistance of the electrochemically active ring at the three-phase boundary of a microelectrode
Δs	local formation entropy of a defect pair
t	time
t_{me}	microelectrode thickness
T	temperature
u	electrical mobility
U	voltage
U_{bias}	dc bias voltage
w	thickness
w_{gb}	grain boundary thickness
$\Delta\tilde{Y}_{gb}$	area-related excess grain boundary conductance
$\tilde{Y}_{gb}$	area-related grain boundary conductance
YSZ	yttria-stabilized zirconia
z	charge number
z_{def}	charge number of the defect
z_{dop}	charge number of the dopant
Z	impedance
3PB	three-phase boundary
ε	permittivity
ε_{bulk}	bulk permittivity
ε_{gb}	grain boundary permittivity
ε_{sc}	space charge permittivity
λ_D	Debye length
μ	chemical potential
$\tilde{\mu}$	electrochemical potential
ρ_{bulk}	bulk resistivity
ρ_{gb}	grain boundary resistivity
σ	conductivity
σ_{bulk}	bulk conductivity
σ_{gb}	grain boundary conductivity
φ	electrical potential
$\Delta\varphi$	space charge potential
ω	angular frequency
ω_r	angular relaxation frequency

Subscripts

bulk	bulk of the material, grain interior
ce	counter electrode
def	defect
dop	dopant
e	electron
eff	effective
el	electrode
eon	electronic charge carrier
gb	grain boundary
h	hole
im	imaginary part
ion	ionic charge carrier
me	microelectrode
RC	resistor in parallel with a capacitor
re	real part
ring	electrochemically active region at the three-phase boundary of a microelectrode
spr	spreading
tot	total
V	vacancy
W	Warburg

1 Introduction

The interdisciplinary field of solid state ionics deals with properties that are related to ionic charge carriers and ionic transport phenomena in solids. It incorporates therefore aspects of solid state chemistry, physical chemistry, solid state physics and materials science. The materials that are investigated in solid state ionics are predominantly ceramics, to be specific inorganic ionic compounds such as crystalline AgCl, NaCl, LaF_3, ZrO_2, SnO_2, $SrTiO_3$, $LaMnO_3$, $LiCoO_2$, Li_4SiO_4, $BaCeO_3$, CuBr or Nasicon ($Na_{1+x}Zr_2P_{3-x}Si_xO_{12}$), and amorphous $(Li_2O)_x(Na_2O)_y(B_2O_3)_{1-x-y}$, or $(AgPO_3)_{1-x}(AgI)_x$ [1–5]. Important phenomena and properties that receive attention are i) ionic conductivity and diffusion in solids; ii) chemical and electrochemical reactions on or in ionic compounds (e.g. oxidation, intercalation, sintering, corrosion); and iii) physics and chemistry of defects in ionic solids. Solid state ionics is thus concerned with the basics of many technologically relevant processes, such as the fabrication and degradation of ceramic materials. However, it is the use of ionic solids in several key technologies, for example in fuel cells, sensors and batteries, which explains the considerable interest in this field during the last ten or twenty years:

i) Fuel cells are considered to play an important role in future electrical-power generation for stationary power supply, vehicles, and portable electrical appliances [6–13]. There are several fuel cell concepts using different electrolytes, of which solid oxide fuel cells (SOFCs) are certainly one of the most promising,

particularly for stationary power supply. SOFCs are based on an ion-conducting oxide (e.g. Y-doped ZrO_2), and research directed towards new solid electrolytes, advanced electrode materials, or improved electrochemical performance of the cells yields important contributions to the field of solid state ionics.

ii) Numerous current research activities in solid state ionics are concerned with investigating sensors for gases such as O_2, CO_2, SO_2, NO_x, H_2 or Cl_2 [14–20]. Sensors based on zirconia ceramics are, for example, employed by the automotive industry to control the combustion process.

iii) Li batteries exhibit the highest energy density of all existing batteries and constitute a market of several hundred million dollars [21–26]. Cathodes of rechargeable Li batteries (e.g. $LiCoO_2$) are ionic intercalation compounds into which Li can be incorporated. The investigation of new cathode materials, and an understanding of intercalation mechanisms, are but two topics in battery research related to solid state ionics.

These examples and the general subjects mentioned above illustrate that ion conduction and the electrochemical properties of solids are particularly relevant in solid state ionics. Hence, the scope of this area considerably overlaps with the field of solid state electrochemistry, and the themes treated, for example, in textbooks on solid state electrochemistry [27–31] and books or journals on solid state ionics [1, 32] are very similar indeed. Regrettably, for many years solid state electrochemistry/solid state ionics on the one hand, and liquid electrochemistry on the other, developed separately. Although developments in the area of polymer electrolytes or the use of experimental techniques such as impedance spectroscopy have provided links between the two fields, researchers in both solid and liquid electrochemistry are frequently not acquainted with the research activities of the sister discipline. Similarities and differences between (inorganic) solid state electrochemistry and liquid electrochemistry are therefore emphasized in this review. In Sec. 2, for example, several aspects (non-stoichiometry, mixed ionic and electronic conduction, internal interfaces) are discussed that lead to an extraordinary complexity of electrolytes in solid state electrochemistry.

The main purpose of this contribution, however, is to review recent advances in solid state ionics achieved by means of microelectrodes, i.e. electrodes whose size is in the micrometer range (typically 1–250 μm). In liquid electrolytes (ultra)-microelectrodes are rather common and applied for several reasons: they exhibit a very fast response in voltametric studies, facilitate the investigation of fast charge transfer reactions and strongly reduce the importance of ohmic drops in the electrolyte, thus allowing e.g. measurements in low-conductive electrolytes [33, 34]. Microelectrodes are also employed to localize reactions on electrodes and to scan electrochemical properties of electrode surfaces (scanning electrochemical microscope [35, 36]); further developments refer to arrays of microelectrodes, e.g. for (partly spatially resolved) electroanalysis [37–39], applications in bioelectrochemistry and medicine [40, 41] or spatially resolved pH measurements [42]. Reviews on these and other applications of microelectrodes are, for example, given in Ref. [33, 34, 43–47].

In solid state ionics, on the other hand, microelectrodes are far less commonly used and only recently has the number of studies using microelectrodes increased

noticeably. This might be surprising, since – particularly because of the complexity of the solid electrolytes – there are many different problems in solid state electrochemistry to which microelectrodes could be applied. They are, for example, destined to quantify inhomogeneous bulk conductivities, to detect highly conductive grain boundaries, or to investigate the distribution of the properties of highly resistive grain boundaries. This is detailed in Sec. 3. Interpreting the results of microelectrode measurements on solid electrolytes is by no means straightforward, however. The equations for the local determination of bulk conductivities are well known [48–50]. On the other hand, the theoretical basis for a quantitative analysis of experiments on grain boundaries, and of impedance studies involving electrodes with electrochemically active three-phase boundaries, have been developed only recently [51–54]; these theoretical considerations are discussed in detail in Sec. 4. From an experimental point of view, microelectrode experiments in solid state ionics can be demanding as well: they often yield very high resistances, since many ceramics exhibit rather low conductivities. Furthermore, even very small stray capacitances can generate considerable measurement artefact. In Sec. 5, some experimental aspects of microelectrode experiments on ionic solids are reviewed. Lastly, Sec. 6 is devoted to examples of microelectrode measurements on ionic compounds. An overview is presented which touches upon most of the recent microelectrode literature in solid state ionics. (Measurements with miniaturized electrodes whose size is of the order of millimeters, and scanning-probe microscopy studies using nanometer-sized electrodes, are not considered.) Four experiments are discussed in more detail: i) a study of inhomogenous bulk conductivities due to non-stoichiometry effects in an oxide ($SrTiO_3$); ii) microelectrode experiments in order to determine the distribution of grain boundary properties in an oxide ($SrTiO_3$); iii) measurements for the detection and quantification of highly conductive grain boundaries in a silver ion conductor (AgCl); and iv) an electrode kinetic study of the oxygen reduction reaction on an anion conductor (ZrO_2). These examples are chosen with the aim of giving at least an idea of the variety of scientific problems (bulk, grain boundary and electrode phenomena) treated in solid state ionics. Furthermore, these experiments provide evidence that microelectrodes are very useful tools in tackling solid state electrochemical problems.

2 Charge Transport and Electrochemistry in Ionic Solids

2.1 Defects in Ionic Crystals

2.1.1 Defects and their Notation

Many important phenomena in solid state ionics, such as ionic conduction, gas permeation through dense solids, solid state reactions, high temperature corrosion, or sintering of polycrystals, involve mobile ionic charge carriers. In most crystalline

lattices, however, only point defects such as vacancies (unoccupied lattice sites) or interstitials (ions on non-regular lattice sites) facilitate the transport of ions. In a certain sense, ionic solids are therefore similar to pure water, wherein "defects" (i.e. H_3O^+ and OH^-) are also necessary for an ionic current [55]. Thus, in most cases defects, rather than regular constituents, are the particles relevant in electrical and electrochemical phenomena in ceramics.

For reasons of clarity, a standard notation for defects in ionic solids has been developed (Kröger–Vink notation [56, 57]). The main symbol of the notation indicates whether the defect is a vacancy "V" or an ion, such as "Ag" in AgCl: a subscript denotes the site that the defect occupies, either the regular lattice site (eg. "Ag" in AgCl) or an interstitial site "*i*", and a superscript identifies the relative charges with respect to the perfect lattice. Dots ($^\bullet$) represent positive charges, dashes ($^|$) are used for negative charges, and *x* denotes electroneutrality with respect to the perfect lattice. Hence, a silver vacancy and a silver interstitial in AgCl are $V_{Ag}^{|}$ and $Ag_i^{\bullet}$ respectively, whereas $V_O^{\bullet\bullet}$ denotes an oxygen vacancy in an oxide. In the following sections, the mechanisms that determine the concentration of point defects in ionic solids are discussed, emphasizing the similarities and differences between solid and liquid electrochemistry.

2.1.2 Intrinsic Disorder

Let us first consider a pure ionic solid with negligible impurity concentration. The two most common types of point defects in such solids are vacancies and interstitials. These defects are usually charged relative to the perfect lattice, and in the bulk oppositely charged defects co-exist in order to balance the charge. Two defect combinations mainly occur in ionic lattices: i) Frenkel disorder (Fig. 1a) with vacancies and interstitials of the same ion being the dominating defects (e.g. in AgCl, AgBr, BaF_2, CaF_2; in the case of anionic defects (BaF_2, CaF_2) the term Anti-Frenkel disorder is often used); ii) Schottky disorder with anion and cation vacancies as the predominant defects (e.g. in NaCl, $SrTiO_3$, MgO).

The formation of defects involves the breaking of bonds; in thermodynamic equilibrium, defects can therefore only exist if the endothermic formation enthalpy is counterbalanced by entropic effects. The predominant contribution to this entropy comes from the increasing number of configurations in which the particles can be arranged in a lattice if defects are present. With analytical expressions for this configuration entropy, the mass action law

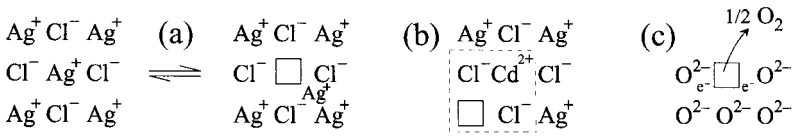

Fig. 1. Defect chemical phenomena: (a) formation of a silver vacancy and an interstitial silver ion in AgCl; (b) formation of a silver vacancy in AgCl by doping with $CdCl_2$; (c) non-stoichiometry in an oxide caused by the excorporation of oxygen.

$$c_A c_B = n_A n_B e^{-\Delta g/kT} = n_A n_B e^{-\Delta h/kT} e^{\Delta s/k} \tag{1}$$

can be deduced for two oppositely charged defects of dilute concentration c_A, c_B [58–60]. In Eq. (1) n_A, n_B are the concentrations of sites available for the defects A, B and Δg, Δh, Δs denote the free formation enthalpy, the formation enthalpy and the local formation entropy of a defect pair.

The situation is equivalent to the formation of H_3O^+ (“proton interstitial”) and OH^- (“proton vacancy”) in water where the endothermic formation enthalpy of the water dissociation reaction is also compensated by the gain of configuration entropy [61]. In both cases, defect chemical reactions can be formulated: the dissociation reaction in water

$$H_2O + H_2O \rightleftharpoons H_3O^+ + OH^- \tag{2}$$

corresponds to the Frenkel pair formation reaction

$$Ag_{Ag}^{x} + V_i^{x} \rightleftharpoons Ag_i^{\bullet} + V_{Ag}^{|}. \tag{3}$$

The defect concentration is exponentially related to $\Delta h/T$ (Eq. (1)) and intrinsic defect concentrations can therefore differ greatly. The materials parameter Δh varies between several tens of kJ/mol and some hundred kJ/mol [62–64], and intrinsic defect concentrations at room temperature can be higher than in pure water (e.g in AgBr), but also much lower than one defect per cm^3 (estimated for MgO). Increasing the temperature strongly enhances the defect concentrations and defect mole fractions in the range of a few percent can be reached, e.g. in AgBr near the melting point, or in β-PbF_2 and β-AgI near the transition temperature to the superionic phase (i.e. to a phase with a highly disordered sublattice of mobile ions) [65–68].

2.1.3 Extrinsic Disorder

The defect concentrations in ionic solids can be enhanced by doping with aliovalent ions: if, for example, Cd^{2+} ions replace Ag^+ ions in AgCl, additional positive charges are introduced that are compensated by negative silver vacancies (Fig. 1b). In terms of a defect chemical reaction the doping can be written as:

$$CdCl_2 \rightarrow 2Cl_{Cl}^{x} + Cd_{Ag}^{\bullet} + V_{Ag}^{|}. \tag{4}$$

The doping of a solid is similar to the enhancement of the H_3O^+ or OH^- concentration in water by adding a strong acid or base. However, while in water mobilities of “dopant” ions are frequently similar to those of the native defects H_3O^+ and OH^- [69, 70], dopant ions in solids (e.g. $Cd_{Ag}^{\bullet}$ in AgCl) are almost immobile. This is also why supporting electrolytes (i.e. electrolytes with dissolved “dopants” that enhance the ionic conductivity, but do not influence electrochemical electrode reactions [71, 72], are unknown in solid state electrochemistry.

If the intrinsic defect concentration is much lower than the dopant (or impurity) concentration c_{dop}, electroneutrality requires a defect concentration c_{def} according to

$$c_{\mathrm{def}} = c_{\mathrm{dop}} \left| \frac{z_{\mathrm{dop}}}{z_{\mathrm{def}}} \right| \tag{5}$$

with z_{dop} and z_{def} being the charge numbers of dopant and compensating defect respectively. Such extrinsic disorder occurs particularly at lower temperatures, where the intrinsic concentrations are rather low. In the case of large defect formation enthalpies (e.g. in oxides), the extrinsic disorder prevails even at high temperatures. However, it should be remembered that – as in water – the mass action law of the defect equilibrium (Eq. (1)) is valid even in the extrinsic regime.

2.1.4 Non-Stoichiometry of Solids

Ionic solids can always exhibit certain deviations from their stoichiometric composition. In thermodynamic equilibrium, tin dioxide ($SnO_{2-\delta}$) is oxygen-deficient, whereas cobalt oxide ($Co_{1-\delta}O$) is a metal-deficient compound. In both cases the δ-value depends on the oxygen partial pressure. On an atomistic scale, deviations from the stoichiometric composition again lead to defects: the oxygen deficiency of a binary oxide $MO_{1-\delta}$, for example, may either be due to metal interstital ions ($M_i^{\bullet\bullet}$) or oxygen vacancies ($V_{\mathrm{O}}^{\bullet\bullet}$). The decreased number of oxide ions, however, needs less positive charge to preserve electroneutrality, and hence the cations are partly reduced in such a case. From a charge carrier point of view, this reduction of cations corresponds to the formation of mobile electrons in the band scheme of the solid. In other words, non-stoichiometry not only introduces ionic defects, but also electronic charge carriers (Fig. 1c). This non-stoichiometry has no direct counterpart in water and leads to a manifold of phenomena such as diffusion of (formally neutral) oxygen in an oxide, mixed ionic and electronic conductivity and reduced electromotive forces that distinguish solid state from liquid electrochemistry [30, 73–75].

With respect to the electronic charge carriers in ionic solids, it should be mentioned that semiconductor-like band structures with relatively wide band gaps (for example ca. 3.1 eV in $SrTiO_3$, 7.3 eV in NaCl and 3.2 eV in AgCl [76–78]) can often be found. In these solids, electrons in the conduction band (CB), and holes in the valence band (VB), can be regarded as electronic defects in equilibrium via the reaction

$$e_{\mathrm{VB}}^{x} + h_{\mathrm{CB}}^{x} \rightleftharpoons e_{\mathrm{CB}}^{\prime} + h_{\mathrm{VB}}^{\bullet}. \tag{6}$$

Similar to a Frenkel disorder, or to the dissociation equilibrium in water, a mass action law according to

$$c_e c_h = K_e \tag{7}$$

can be formulated for the electron concentrations in the conduction band c_{e} and the hole concentration in the valence band c_{h} [73, 79].

The extent of non-stoichiometry, i.e. the extent to which a compound can partly be reduced or oxidized, strongly depends on the kind of cation. In $Co_{1-\delta}O$ or $SnO_{2-\delta}$, δ can be of the order of one percent and in several oxides such as $CeO_{2-\delta}$ and $Mn_{1-\delta}O$ even several percent are possible; in Al_2O_3 or MgO, on the other hand, the degree of non-stoichiometry is extremely small [78, 80–82]. Nevertheless, even very small δ-values can determine the charge carrier concentration in a solid, and thus effects such as the kinetics of solid state reactions.

Let us further consider an oxygen-deficient oxide $MO_{1-\delta}$. The equilibrium with the surrounding gas, which determines the stoichiometry, can be written as

$$O_O^x \rightleftharpoons \tfrac{1}{2}O_2 + V_O^{\bullet\bullet} + 2e' \tag{8}$$

and leads to the mass action law

$$c_e^2 c_V \sqrt{(p(O_2)} = K_\delta \tag{9}$$

with c_V and $p(O_2)$ denoting the oxygen vacancy concentration and the oxygen partial pressure. If the defect concentration is solely determined by the non-stoichiometry, Eq. (9) can be used to calculate the partial pressure dependence of c_e and c_V. Owing to the electroneutrality equation, $2c_V$ equals c_e and

$$c_V = \tfrac{1}{2}c_e = \sqrt[3]{K_\delta/4}(p(O_2))^{-1/6} \tag{10}$$

results. Such a $-1/6$ relationship is frequently found in experiments (e.g. in $BaTiO_3$ [83], $SrTiO_3$ [77, 84], SnO_2 [85, 86] or CeO_2 [87, 88]).

2.1.5 Brouwer Diagrams and Frozen-In Profiles

In many ceramics, intrinsic and extrinsic disorder, as well as the disorder due to non-stoichiometry, have to be considered. Independent of the dopant level, the mass action laws of intrinsic disorder, of the e-h equilibrium and of the reaction with the surrounding phase are valid in thermodynamic equilibrium. Together with the electroneutrality equation

$$\left(z_{dop}c_{dop} + \sum_i z_{def,i}c_{def,i}\right) = 0, \tag{11}$$

a system of four equations results. These equations unambiguously define the four defect concentrations c_{V_O}, c_{V_M}, c_e, and c_h in a binary oxide with Schottky disorder ($V_O^{\bullet\bullet}$ and $V_M^{\parallel}$) and given dopant level c_{dop}.

For broad partial pressure regimes, however, only two mobile defects, or one mobile defect and the dopant, play a role in the electroneutrality equation (Eq. (11)). In theses cases simple partial pressure dependences, namely power laws with concentrations being proportional to $p(O_2)^n$, can be calculated (see e.g. Refs. [57, 80, 89, 90]). One example of such a simplified situation has been examined above (Eq. (10)).

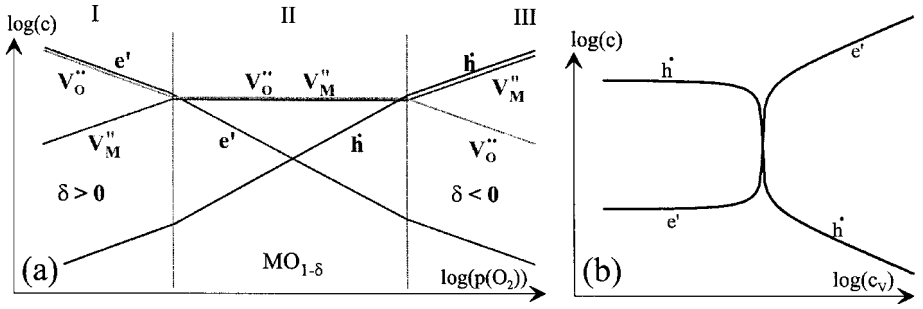

Fig. 2. (a) Sketch of the relations between defect concentrations and partial pressure (Brouwer diagram) of a pure oxide $MO_{1-\delta}$. In regime II the intrinsic Schottky disorder determines the concentration, whereas in I and III non-stoichiometry prevails. (b) Dependence of the hole and electron concentration on the frozen-in oxygen vacancy concentration in a negatively (acceptor) doped oxide.

Considering different pairs of majority defects, all relationships between defect concentrations and partial pressure can be constructed from simplified situations, and this leads to so-called Brouwer diagrams. Figs. 2a and 3a show such Brouwer diagrams for a pure oxide $MO_{1-\delta}$ with Schottky disorder, and for a Schottky-disordered oxide with a negative dopant. (Please notice that the exact curves calculated from the complete electroneutrality equation (Eq. (11)) exhibit smooth transitions rather than sharp bends.)

In the case of a pure oxide (Fig. 2a), three partial pressure regimes are found: the intrinsic regime for medium $p(O_2)$ and two regimes with defect concentrations being dominated by non-stoichiometry. In the case of a doped oxide (Fig. 3a), two different extrinsic regimes have to be distinguished: at low $p(O_2)$ a regime with vacancy-compensated dopant charge (II) and at higher oxygen partial pressure a regime with holes compensating the dopant charge (III).

However, the partial pressures at which the predominant defect(s) change and the width of the different $p(O_2)$ regimes strongly depend on the material under consideration. Frequently, only one or two regimes can be detected in the partial pressure range that is typically used (ca. 10^{-20} bar to 1 bar). In the case of highly doped ZrO_2, which is the electrolyte usually employed in solid oxide fuel cells (SOFCs), only the vacancy-compensated extrinsic regime (II in Fig. 3a) is found [91, 92]; highly doped $LaCrO_3$ (interconnect material in SOFCs) displays the transition from extrinsic vacancy to extrinsic hole compensation (II and III in Fig. 3a) [93, 94]; in nominally pure $CeO_{2-\delta}$ only regimes I and II (Fig. 2a) are observed [87]; and $Fe_{1-\delta}O$ is in its entire stability range metal-deficient ($\delta < 0$) [78]. Defect interactions, however, can lead to deviations from the simple power-laws of Figs. 2 and 3.

It should be emphasized that the kinetics of the equilibration process after a change of the surrounding phase (e.g. a $p(O_2)$ change) requires the movement of defects and can be rather sluggish, particularly at lower temperatures. Therefore, non-equilibrated ionic solids with composition gradients can easily occur, and often the preparation conditions rather than the actual surroundings determine the defect concentrations (frozen-in compositions). On the other hand, internal defect reactions

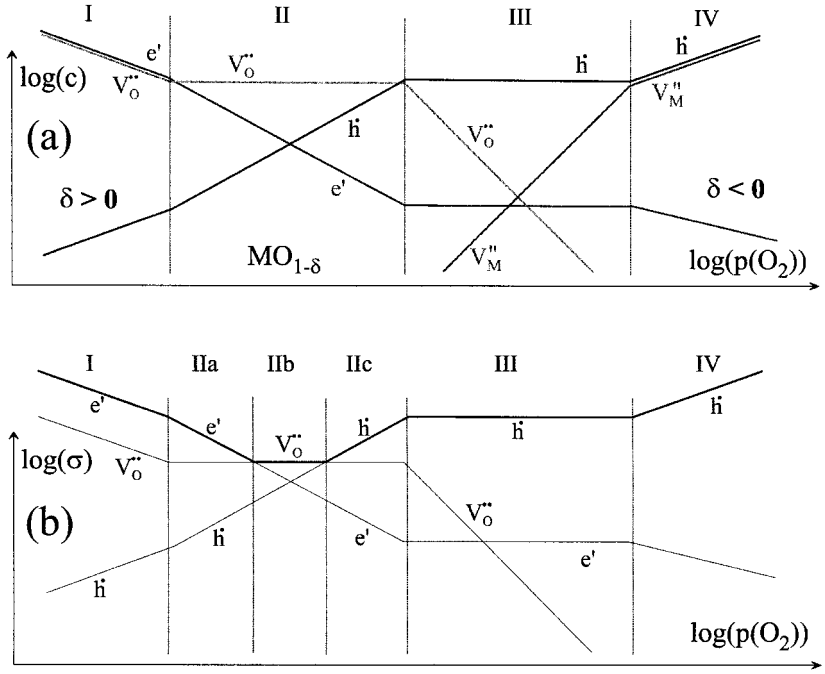

Fig. 3. (a) Sketch of the relations between defect concentrations and partial pressure (Brouwer diagram) of a negatively (acceptor) doped oxide $MO_{1-\delta}$ exhibiting Schottky disorder. Two extrinsic regimes (II and III) and two regimes with prevailing non-stoichiometry (I and IV) are visible. (b) Sketch of the corresponding partial conductivities and the total conductivity (bold line) for $u_e = u_n \gg u_{\text{ion}}$. Oxygen vacancies are assumed to be the only mobile ionic defects. The regime with predominant vacancy concentration is divided into three sub-regimes with electron, vacancy, and hole conduction (IIa, IIb, and IIc).

can be in local equilibrium even if the exchange reaction with the surrounding atmosphere is frozen-in. In particular, the mass action laws of the e-h-equilibrium, and of the Frenkel disorder, can usually be assumed to hold even at low temperatures. In other words, the defect concentrations of, for example, electrons and holes will adjust according to the concentrations of the frozen-in defects.

The dependence of the electronic charge carriers on a frozen-in oxygen vacancy concentration is shown in Fig. 2b. According to this relation, considerable electron and hole concentration gradients can be expected if a vacancy concentration gradient is frozen-in, e.g. due to quenching of the sample during its equilibration process at high temperatures. Oxygen vacancy concentration gradients, and thus c_e and c_h gradients, can also appear if a voltage is applied to ceramics: in an oxide that cannot equilibrate with its surroundings, the oxygen vacancies move in the electrical field, but cannot leave or enter the sample. Consequently, $V_O^{\bullet\bullet}$ accumulate in the vicinity of the cathode, deplete at the anode, and the resulting oxygen vacancy gradient can lead to strong electronic conductivity gradients. This phenomenon plays an important role in the degradation of electroceramic components and spatially resolved mea-

surements of the corresponding conductivity gradients by means of microelectrodes are presented in Sec. 6.2.

2.2 Mass and Charge Transport in Ionic Crystals

In thermodynamic equilibrium, the electrochemical potential of a particle k ($\tilde{\mu}_k = \mu_k + z_k e\varphi$, $\mu_k =$ chemical potential, $\varphi =$ electrical potential, $z_k =$ charge number of the particle, $e =$ elementary charge) is constant. Gradients in $\tilde{\mu}_k$ lead to a particle flux $\mathbf{J_k}$ and from linear irreversible thermodynamics [95] the fundamental transport equation

$$\mathbf{J_k} = -\frac{\sigma_k}{z_k^2 e^2} \nabla \tilde{\mu}_k \tag{12}$$

can be derived. The electrical conductivity σ_k is proportional to mobility u_k and concentration c_k of the mobile charge carrier and is given by:

$$\sigma_k = |z_k| e u_k c_k. \tag{13}$$

A sub-case of Eq. (12) – valid if the chemical potential is constant ($\nabla\mu = 0$) – is Ohm's law, which relates the current density $\mathbf{j_k} = z_k e \mathbf{J_k}$ and $\nabla\varphi$ via

$$\mathbf{j_k} = -\sigma_k \nabla \varphi. \tag{14}$$

Eqs. (12–14) are valid for ionic (vacancies, interstitials), as well as for electronic (electrons, holes), defects. The total conductivity σ_{tot} of an ionic solid is then the sum of ionic and electronic contributions, and both consist of conductivities of different ionic (k,ion) and electronic (m,eon) defects leading to

$$\sigma_{\text{tot}} = \sum_k |z_{k,\text{ion}}| e u_{k,\text{ion}} c_{k,\text{ion}} + \sum_m |z_{m,\text{eon}}| e u_{m,\text{eon}} c_{m,\text{eon}}. \tag{15}$$

Since σ_k is proportional to c_k, the relation between σ_{tot} and the oxygen partial pressure can easily be constructed from the Brouwer diagrams with $|z_k| u_k$ as weighting factors. In Fig. 3b, the conductivities of a doped binary oxide (cf. Fig. 3a) are sketched. The much higher mobility of electronic charge carriers frequently leads to partial pressure regimes (IIa, IIc) in which the total conductivity is dominated by electronic species, although the dopant is mainly compensated by ionic defects. Such regimes are characterized by $\sigma \propto p(\text{O}_2)^{\pm 1/4}$ and are often experimentally observed (e.g. in doped or impurity-dominated $SrTiO_3$ [77, 84, 96], CeO_2 [97, 98], $LaCrO_3$ [93], SnO_2 [86], or $BaTiO_3$ [99]). It is a typical, though not trivial, task in solid state ionics to reconstruct the defect chemistry from $p(\text{O}_2)$-, temperature-, and dopant-dependent conductivity measurements. The great number of ceramic materials, the complication of defect concentrations being partial-pressure-dependent, and the occurrence of mixed ionic and electronic conductivity, are probably why in solid

state electrochemistry bulk (i.e. electrolyte) properties are often the focus of interest; investigations in liquid electrochemistry frequently deal with electrochemical processes at electrodes (“ionics” vs. “electrodics” [100]).

The movement of ionic defects is a thermally activated hopping process and typical activation energies are, for example, 0.03–0.05 eV for $Ag_i^{\cdot}$ in AgCl [101, 102] or $\geq$0.65 eV for $V_O^{\cdot\cdot}$ in various oxides [91, 98, 103–105]. Besides temperature-dependent defect concentrations in the intrinsic regime, this activated hopping process is the main reason for the strong temperature dependence of the conductivity in most ceramic materials (e.g. $\sigma \approx 10^{-1}$ S cm^{-1} in 8–10 mole % Y_2O_3-doped ZrO_2 at 1000 °C, but $\sigma \approx 5 \cdot 10^{-6}$ S cm^{-1} at 300 °C [91, 106, 107]).

2.3 Charge Transport Along and Across Grain Boundaries

Ceramic materials are frequently polycrystalline and their electrical properties are not only determined by the bulk conductivity, but also by the charge transport along and across grain boundaries. From a structural point of view, the grain boundary is a thin region (ca. 0.5–2 nm thick) exhibiting crystallographic and often also chemical differences from the bulk, such as modified lattice distances, enhanced disorder, amorphous regions, segregated impurities or even thin films of a second phase [108, 109]. This structurally modified region is often referred to as the core of a grain boundary [108, 110]. The defect concentration in the core, and thus its electrical properties, can strongly differ from that of the bulk. In ZrO_2 or CeO_2, for example, high grain boundary resistivities are often attributed to siliceous phases at the grain boundaries [111–114]. On the other hand, fast grain boundary diffusion has also been observed in ionic materials [115–117]; this indicates that highly resistive, as well as highly conductive, core regions are possible.

From an electrical point of view, the grain boundary consists not only of its core zone, but also of space charge layers in the adjacent bulk regions with defect concentrations differing from that of the bulk. In order to understand the occurrence of such space charge layers, let us consider a ceramic in the extrinsic regime (negative dopant) with one predominant defect (e.g. oxygen vacancies). In a *Gedankenexperiment*, we introduce a grain boundary into a grain. Owing to the different surroundings, the chemical potential of the mobile charge carrier in the bulk and in the grain boundary core can be expected to be different. Thus, charge carriers begin to move to the region with lower chemical potential. This charge exchange yields net charges in the core and in the adjacent bulk regions (Fig. 4a), and thus an electrical field. Charges move until, in equilibrium, the electrical potential difference balances the chemical potential difference and $\tilde{\mu}$ is constant. The exact charge distribution in the bulk regions follows Poisson’s equation $\mathrm{div}(\mathrm{grad}(\varphi) = -\theta/\varepsilon_{sc}$ (θ = charge density; ε_{sc} = permittivity in the space charge region); the charge is distributed over a zone of typically several nm in thickness, the so-called space charge layer.

With respect to charge transport in space charge layers, two main cases have to be distinguished: decreased charge carrier concentrations, and thus highly resistive space charge layers, and accumulation of charge carriers, i.e. highly conductive space charges. Let us first consider the depletion case. For a spatially constant dopant

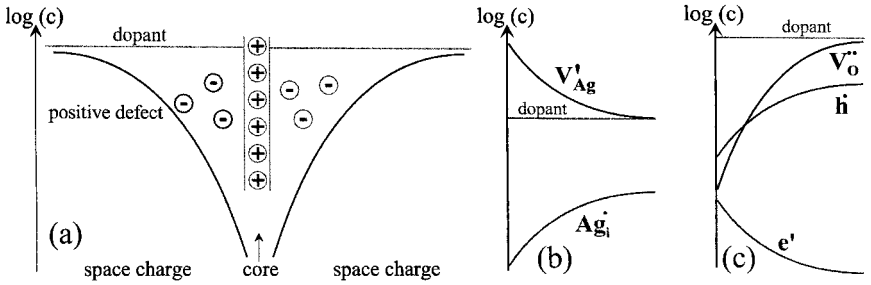

Fig. 4. (a) Model of a grain boundary with a positively charged core region and negative space charges. In the space charge mobile positive defects are depleted. (b) Sketched concentration profiles in a space charge of an extrinsic (positively doped) silver halide. (c) Sketched concentration profiles of majority charge carriers (singly-charged dopant and oxygen vacancies) and minority charge carriers (electrons and holes) in a space charge layer of a negatively (acceptor) doped, mixed conducting oxide.

concentration c_{dop}, the defect concentration in the space charge can easily be calculated from an approximate solution of Poisson's equation leading to the parabolic shape of $\log(c_{\mathrm{def}})$ sketched in Fig. 4a [118]. Concerning the resistance perpendicular to such space charge layers, two limiting cases can be distinguished [118, 119]:

i) If the mean free path of the charge carrier is much smaller than the space charge thickness, the transport through the layer is again governed by the transport equation Eq. (12) [118]. This so-called "drift-diffusion model" applies for ionic defects and is sometimes also discussed for electronic charge carriers, for example for small electron polarons. The approximate small signal ac resistance

$$R_{\mathrm{gb}} = \frac{2\exp(z_{\mathrm{def}} e\Delta\varphi/kT)}{\sigma_{\mathrm{bulk}} A_{\mathrm{gb}}} \sqrt{\frac{\varepsilon_{\mathrm{sc}} k^2 T^2}{2 z_{\mathrm{def}}^2 e^3 c_{\mathrm{dop}} |z_{\mathrm{dop}} \Delta\varphi|}} \tag{16}$$

and capacitance

$$C_{\mathrm{gb}} = \frac{A_{\mathrm{gb}}}{2} \sqrt{\frac{|z_{\mathrm{dop}}| \varepsilon_{\mathrm{sc}} e c_{\mathrm{dop}}}{2|\Delta\varphi|}} \tag{17}$$

as well as the corresponding effective thickness

$$w_{\mathrm{gb}} = 2\sqrt{\frac{2\varepsilon_{\mathrm{sc}}|\Delta\varphi|}{|z_{\mathrm{dop}}| e c_{\mathrm{dop}}}} \tag{18}$$

of such a double space charge layer at a grain boundary can be calculated in straightforward manner [51, 118]. Here the symbol $\Delta\varphi$ denotes the electrical potential difference between the grain boundary core and the bulk interior; A_{gb} is the grain boundary area, and σ_{bulk} represents the conductivity of the grain interior (bulk of the material). In many cases $\varepsilon_{\mathrm{sc}}$ can be approximated by the bulk permittivity $\varepsilon_{\mathrm{bulk}}$.

ii) In the case of electronic charge carriers, the mean free path can be much larger than the space charge thickness and a transfer across the space charge takes place in one step; the charge carriers ''feel'' the energy barrier ($z_{\mathrm{def}} e\Delta\varphi$) rather than the local conductivity [118]. The corresponding ''thermionic emission model'' is often assumed in semiconductors with band conduction such as Si or ZnO [119–121]. Eqs. (17) and (18) are again valid, but the small signal ac resistance follows a modified equation [118]. However, since the drift-diffusion and the thermionic emission model lead to similar I-V and C-V characteristics [118, 119], it can be difficult to decide which of the models should be applied to interpret the experimental results.

The current-voltage (I-V) and capacitance-voltage (C-V) relationships of grain boundaries, however, are rather complicated, since under bias an asymmetric charge redistribution between the core and the two space charge layers takes place. This redistribution depends on the (usually unknown) density and energy of the levels (states) in the core of the grain boundary and complex I-V and C-V characteristics result [121–123]. Ohmic, sub-ohmic ($\mathrm{dlog(I/A)/dlog(U/A)} = \alpha < 1$) and super-ohmic ($\alpha > 1$) regimes can, for example, be observed in a single I-V curve.

In the case of an enhanced charge carrier concentration in the space charge (cf. Fig. 4b), mainly the current parallel to the grain boundary plane is important. The corresponding parallel excess grain boundary conductance

$$\Delta \tilde{Y}_{\mathrm{gb}} \approx 4\lambda_D \sigma_{\mathrm{bulk}} \exp(e\Delta\varphi/2kT) \tag{19}$$

has been deduced in Ref. [124] for $|z_{\mathrm{dop}}| = |z_{\mathrm{def}}| = 1$, with the Debye length λ_D being defined as $\sqrt{(\varepsilon_{\mathrm{sc}} kT)/2e^2 c_{\mathrm{def,\,bulk}}}$. In the case of transport along the grain boundary, the mean free path of the charge carrier plays often no role and Eq. (19) is valid for both ionic and electronic defects. Accumulation space charge layers play an important role in heterogeneous doping of solid ionic conductors (i.e. the addition of a non-soluble insulating compound, e.g. Al_2O_3 in AgCl) [125–127].

The majority charge carrier determines the electrical potential profile in a space charge layer, but the minority charge carriers are also in thermodynamic equilibrium, and thus their concentrations adapt to the given electrical potential. Consequently, in an oxide with a negative dopant and oxygen vacancy depletion, holes are depleted as well, whereas the electron concentration is enhanced in the space charge (Fig. 4c). It is also worth mentioning that, although dopants exhibit a very low mobility and do not contribute to the ionic current, they can equilibrate at high temperatures and frequently display concentration profiles in space charge layers [128]. If the majority charge carrier is depleted, then the dopant concentration is enhanced in the space charge region; this is often referred to as ''segregation of the dopant''.

2.4 Electrical Transport and Electrochemical Reactions at Electrode/Solid Interfaces

In the case of electrical transport across and along space charge layers at grain boundaries, there is usually no fundamental difference between electronic and ionic charge carriers. At electrodes, however, electrons and ions behave completely differ-